*Cerebral Cortex*, 2021;00: 1–13

https://doi.org/10.1093/cercor/bhab251
Original Article



ORIGINAL ARTICLE

# Articulatory Gain Predicts Motor Cortex and Subthalamic Nucleus Activity During Speech

C. Dastolfo-Hromack[1], A. Bush[2,3], A. Chrabaszcz[4], A. Alhourani[5], W. Lipski[6], D. Wang[9], DJ Crammond[6], S Shaiman[1], MW Dickey[1], LL Holt[7], RS Turner[8], JA Fiez[4] and RM Richardson[2,3]

[1]Department of Communication Science and Disorders, University of Pittsburgh School of Health and Rehabilitation Sciences, Pittsburgh, PA 15260, USA, [2]Department of Neurological Surgery, Massachusetts General Hospital, MA 02114, USA, [3]Harvard Medical School, Boston, MA 02115, USA, [4]Department of Psychology, University of Pittsburgh, Pittsburgh, PA 15260, USA, [5]Department of Neurosurgery, University of Louisville, Louisville, KY 40292, USA, [6]Department of Neurological Surgery, University of Pittsburgh School of Medicine, Pittsburgh, PA 15213, USA, [7]Department of Psychology, Carnegie Mellon University, Pittsburgh, PA 15213, USA, [8]Department of Neurobiology, University of Pittsburgh School of Medicine, Pittsburgh, PA 15213, USA and [9]School of Medicine, Tsinghua University, Beijing 100084, China

Address correspondence to R. Mark Richardson, Department of Neurosurgery, Massachusetts General Hospital, 55 Fruit St., Boston, MA 01224, USA. Email: mark.richardson@mgh.harvard.edu

## Abstract

Speaking precisely is important for effective verbal communication, and articulatory gain is one component of speech motor control that contributes to achieving this goal. Given that the basal ganglia have been proposed to regulate the speed and size of limb movement, that is, movement gain, we explored the basal ganglia contribution to articulatory gain, through local field potentials (LFP) recorded simultaneously from the subthalamic nucleus (STN), precentral gyrus, and postcentral gyrus. During STN deep brain stimulation implantation for Parkinson's disease, participants read aloud consonant-vowel-consonant syllables. Articulatory gain was indirectly assessed using the F2 Ratio, an acoustic measurement of the second formant frequency of/i/vowels divided by/u/vowels. Mixed effects models demonstrated that the F2 Ratio correlated with alpha and theta activity in the precentral gyrus and STN. No correlations were observed for the postcentral gyrus. Functional connectivity analysis revealed that higher phase locking values for beta activity between the STN and precentral gyrus were correlated with lower F2 Ratios, suggesting that higher beta synchrony impairs articulatory precision. Effects were not related to disease severity. These data suggest that articulatory gain is encoded within the basal ganglia-cortical loop.

**Key words:** basal ganglia, local field potential, motor cortex, movement gain, speech

## Introduction

Articulatory gain is the increase or decrease in speech movement excursion of articulators that determines whether articulation is precise (i.e., clear speech) or imprecise (i.e., mumbling). Deficits in articulatory gain often occur in Parkinson's disease (Sapir et al. 2010; Sapir 2014; Guenther 2015; Behroozmand et al. 2018), implicating the basal ganglia-cortical loop in this process. Few studies have directly measured basal ganglia neural activity during speech production (Hebb et al. 2012; Hohlefeld et al. 2017; Lipski et al. 2018; Tankus et al. 2018; Chrabaszcz et al. 2019; Tankus and Fried 2019), none of which have examined the neurobiological correlates of articulatory gain. Due to this knowledge gap, articulatory gain is not adequately accounted for in neurobiological theories of speech motor control (Hickok 2012; Guenther 2015), limiting efforts to develop treatments that

**Table 1** Participant demographic characteristics

| Subject | Gender | Age | Handedness | Education, years | Duration of disease, years | Hoehn and Yahr stage | UPDRS Score |
|---|---|---|---|---|---|---|---|
| 1 | Male | 71 | n/a | n/a | 6 | 2 | 35 |
| 2 | Male | 60 | Right | 12 | 14 | n/a | 53 |
| 3 | Female | 53 | Left | 12 | 22 | n/a | 26 |
| 4 | Male | 69 | Right | 14 | 9 | 2 | 46 |
| 5 | Male | 61 | Right | 16 | 5 | 2 | 31 |
| 6 | Male | 68 | Left | 16 | 8 | 2 | 50 |
| 7 | Male | 57 | n/a | n/a | 7 | 2 | 44 |
| 8 | Male | 82 | Right | 16 | 8 | n/a | 36 |
| 9 | Male | 66 | Right | 19 | 7 | 2 | 45 |
| 10 | Female | 71 | Right | 16 | 8 | n/a | 24 |
| 11 | Male | 77 | Right | 18 | 10 | n/a | 27 |
| 12 | Male | 60 | Right | 13 | 6 | 2 | 39 |

ameliorate articulatory gain disorders and improve patients' quality of life.

Theories of speech production presume that speech operates by means of a neural network (Houde and Nagarajan 2011; Hickok 2012; Guenther 2015; Behroozmand et al. 2018), the anatomic nodes of which have been explored primarily by functional neuroimaging, but also by electrocorticography (ECoG). The precentral gyrus inherently is involved in articulatory gain, as it is critical for speech production (Soros et al. 2006; Eickhoff et al. 2009; Behroozmand et al. 2015) and contains a somatotopic organization for the speech articulators (Bouchard et al. 2013; Conant et al. 2014; Bouchard and Chang 2014a, 2014b; Bouchard et al. 2016; Chrabaszcz et al. 2019). Theoretical studies, as well as studies in patients implanted with deep brain stimulation (DBS) leads, also have highlighted the basal ganglia as an important node in the speech motor control network (Murdoch 2001; Bohland et al. 2010; Martel Sauvageau et al. 2015; Aldridge et al. 2016). Evidence from studies of limb motor control implicates the basal ganglia in movement gain (Turner and Desmurget 2010). Given that neural activity in the subthalamic nucleus (STN) is differentially modulated by specific articulators (Chrabaszcz et al. 2019), we hypothesized that measures reflecting aspects of articulatory gain may be encoded in LFPs generated in the STN and precentral gyrus.

We developed an intraoperative protocol requiring patients to read single words and pseudowords aloud during awake DBS implantation surgery, while capturing electrophysiological recordings simultaneously from both the sensorimotor cortex and STN. We defined articulatory gain as the ratio of the second formant frequencies in the patients' production of the vowels/i/and/u/(F2 Ratio). This measure has both theoretical and clinical relevance, as was first proposed by Sapir et al. (2010, 2007). Formant frequencies represent frequency regions of increased intensity in the speech spectrum during vowel production, which contribute to accurate speech perception (Kent and Read 2002). Multiple formants exist, but the second formant (F2) is most related to anterior–posterior tongue movements (i.e., tongue excursion) during vowel production (Kent et al. 1999). Because of this relationship to tongue position changes, the F2 Ratio has been shown to differentiate between Parkinsonian speech, characterized by reduced articulatory excursion, and normal speech (Sapir et al. 2010), demonstrating its validity for operationalizing articulatory gain. In addition, one internal model of speech production (Perkell et al. 1997; Perkell 2012) proposes that acoustic variables (i.e., formant frequencies) are fundamental goals of articulatory movements. By examining the neural signal simultaneously recorded from multiple cortical regions and the STN, we demonstrate that changes in articulatory gain are associated with specific cortical-basal ganglia network dynamics.

## Methods

### Subjects

Intraoperative recordings were obtained from patients with Parkinson's disease (Table 1) undergoing awake stereotactic implantation of DBS leads in the STN; all participants were native-English speakers. All procedures were completed with the informed written consent of participants, in accordance with a protocol approved by the University of Pittsburgh Institutional Review Board (PRO13110420). Dopaminergic medication was withdrawn overnight before surgery. Patients underwent standard preoperative evaluations that included the Unified Parkinson's Disease Rating Scale (UPDRS) within 4 months prior to surgery. Data from these subjects were also used in a previously published study (Chrabaszcz et al. 2019).

### Behavioral Paradigm

Participants were visually cued to read aloud a consonant-vowel-consonant (CVC) utterance consisting of words and pseudowords, which were printed on a black screen and written in white lettering (Fig. 1). Stimuli were balanced on psycholinguistic parameters (for a detailed description, see [Moore et al. 2017]). Participants were encouraged to produce the word as soon as the text appeared on the screen. Matlab software (MathWorks, Natick, MA, USA) and Psychophysics Toolbox extensions (Brainard, 1997; Pelli, 1997; Kleiner et al. 2007) were used to create the visual stimuli. All patients underwent presurgical practice with the task to optimize patient performance and ensure adequate understanding of instructions. Participants performed between 2 and 4 sessions, with 120 trials in a session. One trial consisted of one word or pseudoword.

### Cortical Recordings

ECoG recordings were collected during surgery using a temporary subdural electrode strip, targeted to the ventral sensorimotor cortex. The safety of this technique has been

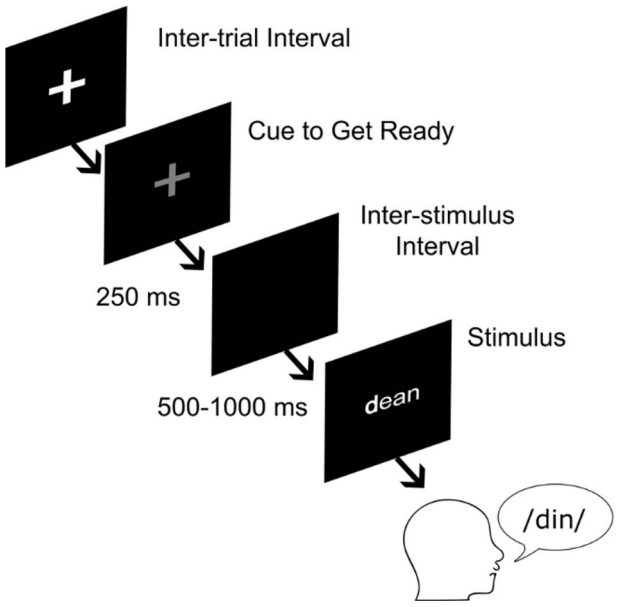


**Figure 1.** Task overview. During awake surgical implantation of deep brain stimulation leads, participants were presented with written stimuli and were asked to read the stimuli aloud. Spoken word is expressed through the International Phonetic Alphabet.

described in 2 prior reports that represent a combined experience in over 500 subjects (Panov et al. 2017; Sisterson et al. 2021). Recordings were collected using the Grapevine neural interface processor (Ripple LLC, Salt Lake City, UT, USA) at a sampling rate of 30 kHz. The electrode strip was inserted through the burr hole after opening the dura. The majority (10) of electrode strips were either 6 or 28 channel Ad-Tech electrode strips (Ad-Tech Medical Corporation, Racine, WI, USA); however, 2 subjects were implanted with 36 and 54 PMT electrode strips (PMT Corporation Chanhassen, MN, USA). Analysis was limited to electrodes which covered the precentral or postcentral gyri ($n = 180$). Electrode recording locations were determined from reconstructions using intraoperative fluoroscopic images, coregistered preoperative and postoperative computed tomography (CT) images and preoperative magnetic resonance imaging (MRI) scans following procedures described in (Randazzo et al. 2016). The Randazzo localization method was validated using a functional mapping of electrode activation and inter-rater reliability procedures. Procedures were validated by 3 independent reviewers and spatial location was verified by functional analysis in motor cortex. The technique utilizes an intraoperative fluoroscopic image to accurately align the pre and postoperative images. The CT scan and preoperative MRI were coregistered using mutual information available on both images within SPM software. The CT and MRI images were then rendered into a 3D skull and brain using Osirix and Freesurfer software. These surfaces were then uploaded into a custom Matlab user interface with the intraoperative fluoroscopy image and aligned using common landmarks such as implanted electrodes, stereotactic frame pins, and skull outline. Localization of electrodes into patient native space was conducted using the Freesurfer suite (Dale et al. 1999) (http://surfer.nmr.mgh.harvard.edu/) and a custom-made graphical user interface in MATLAB. These localizations were then registered into the Montreal Neurological Institute (MNI) common space template using Brainstorm (Tadel et al. 2011) (https://neuroimage.usc.edu/brainstorm/). Recording locations were manually assigned to precentral gyrus or postcentral gyrus based on native space anatomy, utilizing the central sulcus as the primary demarcating landmark.

## STN Recordings

Electrophysiological recordings were completed prior to bilateral DBS lead implantation. LFPs were recorded using the Neuro-Omega recording system and Parylene insulated, microphonic-free tungsten macroelectrodes (0.55 mm in diameter, 1.4 mm in length). The macroelectrodes were located 3 mm above the high impedance contact of each microelectrode. Anatomical locations of macroelectrode recordings were expressed in terms of the microelectrode recording-defined STN boundaries along each electrode trajectory. Recordings were obtained from a total of 88 sites across all patients. Each recorded session represents a different depth within the STN. The microelectrodes were oriented using 2–3 trajectories: central trajectory plus posterior and/or medial trajectories. Thus, each macroelectrode recording location was identified by its relative position within the recording orientation (central, posterior, or medial) and the percent depth through the physiologically defined STN within that trajectory (with 0% representing the ventral STN boundary and 100% representing the dorsal STN boundary). LFP signals were band-pass filtered at 0.075–400 Hz and digitized at 1375 Hz. Recording trajectories through the STN were reconstructed using the Lead-DBS toolbox in Matlab (Horn and Kühn, 2015), based on identification of lead contacts in postoperative CT scans (Fig. 2). Coregistration and normalization were completed using MNI coordinates.

## Audio Recording and Editing

Speech samples were recorded using an omnidirectional microphone to limit distortion effects (Audio-Technica, Stow, OH; model ATR3350iOS, frequency response 50–18 000 Hz; 4 participants: Presonus, Baton Rouge, LA model PRM1 Precision Flat Frequency Mic, frequency response 20–20 000 Hz). The microphone was oriented at an angle of approximately 45° and a distance of approximately 8 cm to the participant's mouth. For synchronization to the neural data, digital pulses were delivered to both the Grapevine neural processor (digitized at 30 kHz) and Neuro-Omega and labeled with digital pulse events at the onset of each trial. Digital pulses were delivered through a USB data acquisition unit (Measurement Computing, Norton, MA model USB-1208FS).

## Calculation of F2 Ratio

Articulatory gain was operationalized using the F2 Ratio, which represents an estimation of anterior to posterior tongue movement (Kent et al. 1999; Sapir et al. 2007; Sapir et al. 2010) and is calculated by the mean second formant frequency of/i/divided by the mean second formant frequency of/u/ (Fig. 3). The second formant frequency was extracted from a time window that covered the middle one-third of selected vowels using the Burg algorithm in Praat (Boersma and Weenink 2019). Second formants were extracted only from/u/and/i/productions (Fig. 1B). Extractions were automatized using a custom Praat script and verified post hoc by a speech language pathologist. Means were calculated by averaging the second formant from all instances of the respective vowels within a single session. Second formant

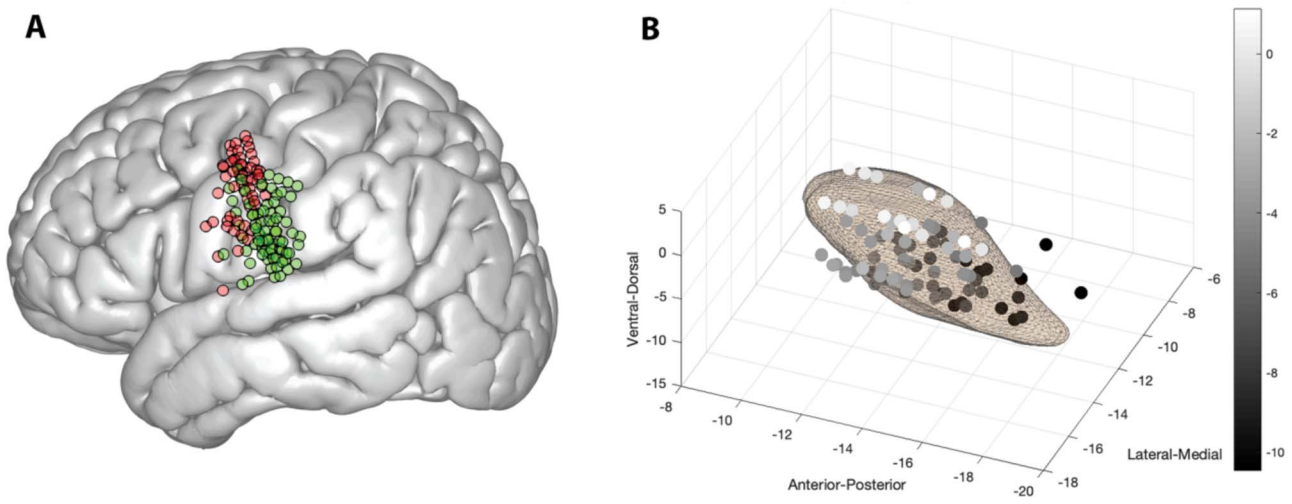


**Figure 2.** Recording locations. (*A*) Cortical recording locations in precentral gyrus represented in red dots, and postcentral gyrus represented in green dots. Note that one subject is not represented here in common space because transformation to MNI space could not be completed due to low imaging quality. (*B*) Subthalamic nucleus recording locations in MNI coordinates. Depth, as represented in MNI coordinates, is depicted in greyscale to highlight depth differences.

means were then divided to determine the F2 Ratio for a session. Each trial consisted of a stimulus with a single vowel which limited the F2 Ratio analysis to a session level statistic rather than trial level. Because the F2 Ratio measurement requires 2 vowels (/i/and/u/), the measurements were averaged across multiple productions within a session. Averaging across session was also completed to mitigate the effects of phonetic context on the second formant (Stevens and House 1963; Hillenbrand et al. 2001; Lee et al. 2005; Strange et al. 2007; Chladkova et al. 2011; Slis and Van Lieshout 2013), which was highly variable across stimuli (Supplementary Fig. 2). Without averaging across session, the measurement would not reflect articulatory gain, but rather phoneme identity. The final F2 Ratio measurement represents an indication of articulatory gain for a subject for a particular session.

## Data Selection

Trials were only included for analysis if the trial phonemes could be clearly transcribed by the speech language pathologist, a subject's produced utterance matched the stimuli's targeted CVC structure, and a subject's response included the stimuli's targeted phonemes. On the basis of these criteria, 359 (9.8%) out of a total of 3669 recorded trials were rejected. See Table 2 for more details.

## Data Processing

An overview of data processing steps can be found in Supplementary Figure 1. All electrophysiological data were processed in MATLAB using custom scripts, the Statistical Parametric Mapping (SPM12) (Wellcome Department of Cognitive Neurology, London, UK) and Fieldtrip (Oostenveld et al. 2011) toolboxes. Data were resampled to a sampling rate of 1 kHz, and cardioballistic effects and line noise were removed using a 1 Hz high pass filter and 58–62 Hz notch filter. To minimize noise and ensure recordings were comparable across acquisition environments, LFP signals were re-referenced offline to a common average reference, which was applied over blocks of electrodes connected by the same headstage connector for the ECoG recordings and a standard procedure for STN recordings (common average reference). Residual artifacts and excessive noise were removed by visual inspection, leading to a rejection of 4.8% of the data. For spectral decomposition, a Morlet wavelet transformation was completed with 7 cycles over frequencies between 1 and 200 Hz in increment steps of 2 Hz with a time resolution of 40 ms. Signal amplitude (power) was extracted from canonically defined EEG frequency bands: theta (4–8 Hz), alpha (8–12 Hz), beta (12–35 Hz), low gamma (50–90 Hz) (Lofredi et al. 2018) and high gamma (80–110 Hz) (Crone et al. 1998; Ray et al. 2008). The signals were then normalized to baseline using a z-score method; the baseline period was 1 s long (250 ms before and 750 ms after green cross presentation). Normalization equation is below, $x = signal$.

$$\frac{(x - Mean_{baseline})}{SD_{baseline}} \quad (1)$$

## Statistical Analysis

All analyses were conducted in MATLAB 2017a (Mathworks Inc., Natick, MA, USA), R version 3.4.4 (R Development Core Team, 2018) and Praat (Boersma and Weenink 2019). A between-subject and session design was utilized to examine naturally occurring differences in articulatory gain between subjects and sessions.

Electrophysiology data were imported into R (R Development Core Team, 2018), then downsampled to 120 ms segments across the speech task to conduct the following analyses: For the cortical data, LFP power values were averaged across electrodes in 2 regions of interest (ROIs): (1) the precentral gyrus and (2) the postcentral gyrus. Downsampling and averaging were performed after spectral decomposition to avoid smearing of frequency content. We performed the ROI analysis instead of an electrode-level analysis because the F2 ratio variance came from across subjects and sessions, but the exact electrode locations varied from subject to subject, making it impossible

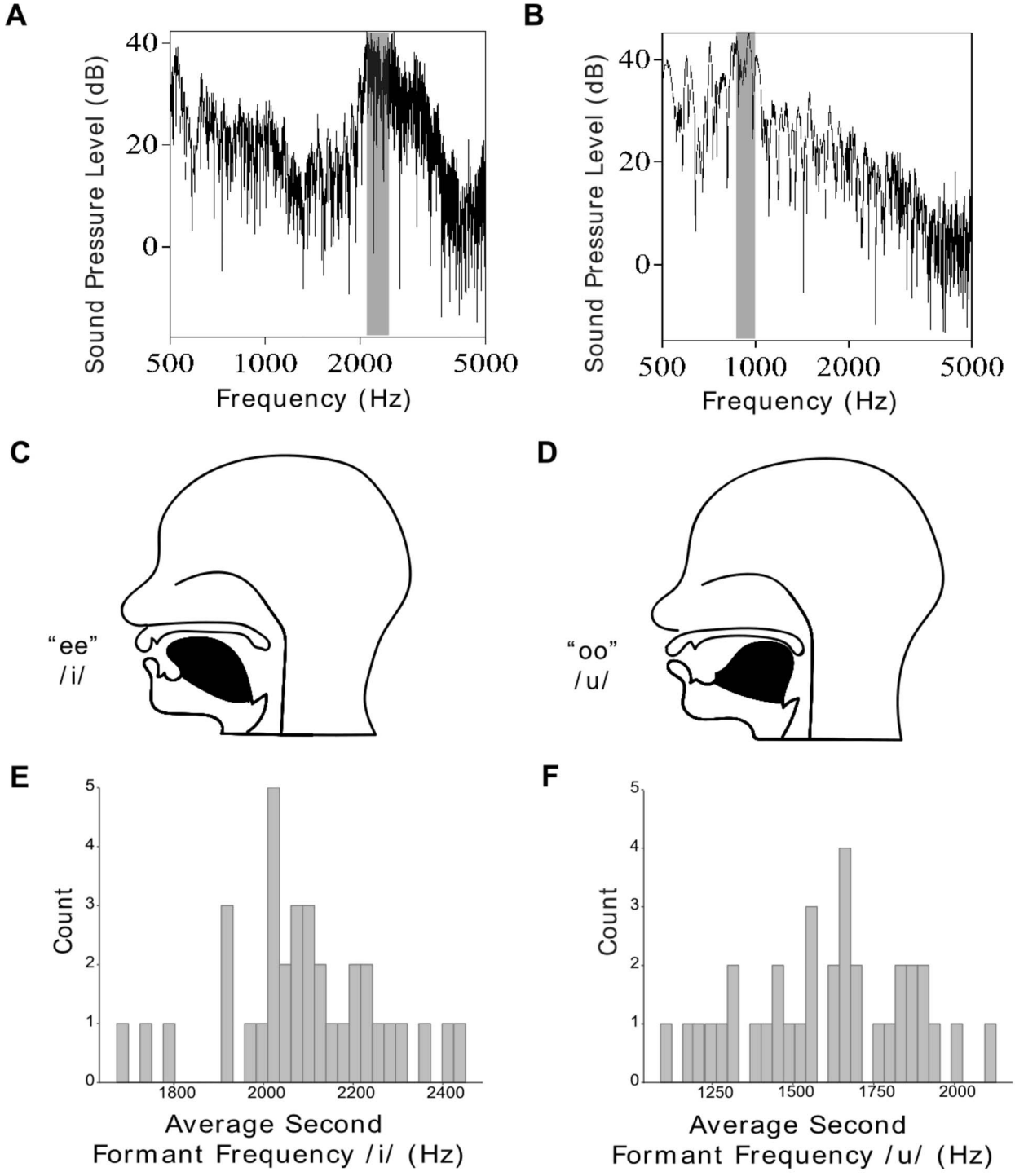


**Figure 3.** Second formant frequency ratio (F2 Ratio) captures speech gain. (A) Power spectrum of the vowel/i/(as in "he"). (B) Power spectrum of the vowel/u/(as in "who"), gray highlighting demonstrates the peak of the second formant (F2). The ratio of F2 of/i/vs. F2 of/u/provides an estimate of anterior to posterior tongue movement. In this example, the F2 of/i/is approximately 2100 Hz, and the F2 of/u/is 900 Hz, yielding a high formant ratio of 2.3 (2100/900), characteristic of clear speech. (C) Schematic of the tongue position during/i/production. (D) Schematic of the tongue position during/u/production. The difference between these positions is captured by the F2 Ratio because the F2 lowers as the tongue moves more posteriorly in the oral cavity. E. and F. Histograms of the averaged F2 gathered from each session. Participants produced F2 Ratios between 1.05 and 1.87.

**Table 2** Data inclusion and subjects' performance characteristics

| Subject | Cortical recording | Number of cortical electrode contacts | STN recording | Number of STN electrode contacts | Rejected trials, % | Speech latency (SD), sec. | Speech duration (SD), sec. | F2 Ratio (mean across sessions) | No. of sessions |
|---|---|---|---|---|---|---|---|---|---|
| 1 | Yes | 6 | Yes | 6 | 34.2 | 1.24 (0.28) | 0.63 (0.13) | 1.18 | 2 |
| 2 | Yes | 28 | Not used | Not used | 20.8 | 1.53 (0.41) | 0.83 (0.29) | 1.05 | 2 |
| 3 | Yes | Not used | Yes | 6 | 6.1 | 1.36 (0.61) | 0.52 (0.12) | 1.06 | 2 |
| 4 | Yes | 6 | Yes | 12 | 4.5 | 1.07 (0.98) | 0.58 (0.09) | 1.17 | 4 |
| 5 | Yes | 54 | Yes | 6 | 4.2 | 0.77 (0.15) | 0.64 (0.16) | 1.87 | 2 |
| 6 | Yes | 28 | Yes | 6 | 4.6 | 0.75 (0.16) | 0.60 (0.16) | 1.26 | 2 |
| 7 | Yes | 6 | Yes | 6 | 5 | 0.86 (0.19) | 0.47 (0.10) | 1.68 | 2 |
| 8 | Not used | Not used | Yes | 9 | 22.3 | 2.75 (1.94) | 0.44 (0.08) | 1.12 | 3 |
| 9 | Yes | 28 | Yes | 12 | 2.1 | 0.66 (0.22) | 0.61 (0.13) | 1.44 | 4 |
| 10 | Yes | 6 | Yes | 6 | 8.6 | 1.29 (0.58) | 0.84 (0.23) | 1.49 | 3 |
| 11 | Not used | Not used | Yes | 4 | 12.7 | 1.33 (0.49) | 0.54 (0.13) | 1.37 | 2 |
| 12 | Yes | 36 | Yes | 12 | 7.1 | 1.00 (0.86) | 0.44 (0.10) | 1.23 | 4 |

to correlate the F2 ratio with the signal at each individual electrode. Signals in the STN were also averaged for each of the central, posterior, and medial trajectories within a session. All electrodes were included in analysis based on recent statistical recommendations cautioning the practice of electrode selection by neural activation (Kriegeskorte et al. 2009) and the possibility of atypical neural patterns contributing to motor control processes (Eusebio and Brown 2009; Little et al. 2019).

Initial qualitative inspection of the neural data was completed by examining the power spectrum surrounding the time of vowel onset (from $t_1 = -40$ ms to $t_2 = 160$ ms relative to vowel onset), across varying levels of F2 Ratio performance. The power spectrum was calculated on session level data. A linear model was conducted across frequencies of the power spectrum, predicting normalized power from the frequency and F2 Ratio, within a fixed time window (Equation 2). To descriptively analyze differences in power across F2 Ratio, the highest and lowest F2 Ratios observed in behavioral performance were then used to calculate predicted power across frequencies in each region of interest. For all equations, Z = z-scored neural power, $f$ = frequency, $t$ = time, $\beta_0$ = intercept, and $\beta_1$ = main effect.

$$Z_{[t_1,t_2]}(f) = \beta_0(f) + \beta_1(f) \times (F2\ Ratio) \quad (2)$$

For the primary hypothesis that F2 Ratio would predict neural power, a mixed effects model with neural band, F2 Ratio and their interaction as independent variables and neural power as the dependent variable was computed. A model was completed at 2 separate time segments within each brain region of interest, before speech production and during speech production. These time segments were chosen to account for the possibility of an articulatory gain relationship existing both during movement preparation and execution. Subject was modeled as a random intercept in order to account for data arising from multiple subjects and a random slope of session was included. For all mixed effect models, $\gamma_0$ = intercept, $\gamma_1$, $\gamma_2$, $\gamma_3$ = main effects, $u$ = error due to intersubject differences, and $e$ = unexplained error.

$$Z_{ij} = \gamma_0 + \gamma 1(F2\ Ratio) + \gamma 2(band) + \gamma 3(F2\ Ratio\ X\ band) + (u_{0j} + e_{ij}) \quad (3)$$

Recommended procedures to ensure the most parsimonious model were followed for all mixed effects models (Matuschek et al. 2017). To determine the overall interaction effect of band and F2 Ratio, a type III analysis of variance was run on the mixed effects model summary for each model, and $P$ values were false discovery rate (FDR) corrected within brain region (2 models within a region) using the Benjamini and Yekutieli (2001) procedure. Because the same hypothesis was tested in 3 different brain regions, a Bonferroni adjusted significance level (alpha = 0.0167) was used to account for familywise error. Simple slopes with pairwise contrasts were extracted from these models to determine the bands driving the significant prediction of F2 Ratio to neural power. Mixed effects models were conducted using the lme4 and lmerTest packages in R and simple effects (slopes) were extracted using the function simple_slopes in the CRAN package "reghelper".

To control for effects related to Parkinson's disease severity (UPDRS scores) and physiologically defined depth in the STN, mixed effect models were conducted to predict power from these factors:

$$Z_{ij} = \gamma_0 + \gamma 1(UPDRS\ or\ depth) + \gamma 2(band) + \gamma 3(UPDRS\ or\ depth\ X\ band) + (u_{0j} + e_{ij}) \quad (3)$$

To measure functional connectivity between STN and cortex, a phase locking value (PLV) was calculated at each time point (10 ms intervals) and frequency for each STN-cortical contact pair using Fieldtrip toolbox, where amplitude normalized cross-spectral densities between paired complex signals were divided by their respective auto-spectral densities (Lachaux et al. 1999). Similarly, averaged PLVs were then extracted from standard frequency bands for each channel pair. To examine the correlation of STN-cortical functional connectivity with the F2 Ratio, averaged STN-precentral gyrus PLV was obtained for each subject in each frequency range by averaging PLVs across time points from stimulus onset to speech offset, across all STN-precentral gyrus contact pairs, and across all sessions. The equation for obtaining PLV is included below. This defines the PLV between signals $i$ and $j$ at time $t$ and frequency $f$, where $N$ is the number of trials and $\varphi_{f,i}(t,n)$ is the instantaneous phase of signal $i$ in trial $n$ at time $t$.

$$PLV_{f,i,j}(t) = \frac{1}{N}\left|\sum_{n=1}^{N} e^{-i\left(\varphi_{f,i}(t,n) - \varphi_{f,j}(t,n)\right)}\right| \quad (6)$$

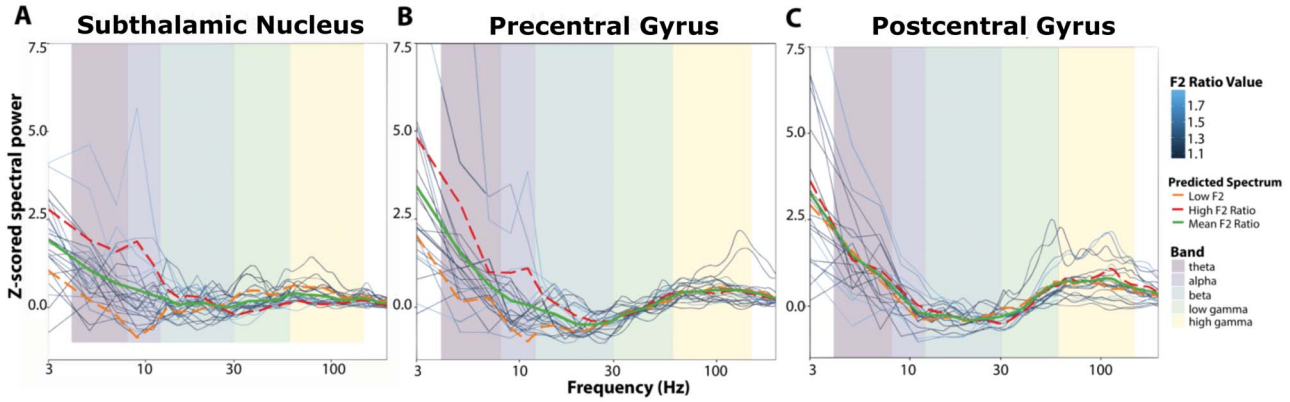


**Figure 4.** Local field potential spectral power across frequencies around vowel onset as a function of formant ratio (F2 Ratio). (*A*) In the 200 ms surrounding vowel onset, the z-scored spectral power was predicted by a linear model using F2 Ratio as a predictor (see Equation 2) in the subthalamic nucleus. (*B*) Linear model predicting F2 Ratio in the precentral gyrus and (*C*) Linear model predicting F2 Ratio in the postcentral gyrus. In all figures, raw neural data are shown in the blue lines, color coded by corresponding F2 Ratio. Predicted spectral data are displayed in orange, red, and green to demonstrate patterns in variation as a function of speech gain (F2 Ratio) (see methods for details). Frequency bands are outlined in pastel colors to denote cut offs for the canonical frequency bands utilized in further analysis (Figs 5 and 6).

Averaged STN-post central gyrus PLVs were obtained in a similar way. A total of 10 subjects were used for this comparison. A series of linear models were then conducted across frequencies, predicting STN-precentral gyrus PLV or STN-postcentral gyrus PLV from the F2 Ratio:

$$PLV(f) = \beta_0(f) + \beta_1(f) \times (\text{F2 Ratio}) \quad (7)$$

To assess for the effect of participant age and disease status, the PLVs were correlated to UPDRS score and age using the spearman correlation. Correction for FDR was applied to control for multiple comparisons and alpha was set at 0.05 for PLV analysis.

## Results

### Subjects and Behavioral Performance

Data were collected in 12 native-English speaking subjects with Parkinson's disease undergoing STN DBS implantation with simultaneous research ECoG recordings. Subject demographics and clinical characteristics are shown in Table 1, and their behavioral performance is shown in Table 2. Participant age ranged from 53 to 82 (mean = 66 years) with an average UPDRS score of 38. Average duration of speech production was 595 ms (SD = 131 ms), and average F2 Ratio was 1.32 (SD = 0.25). Test–retest reliability was calculated for the F2 Ratio by correlating the first and second sessions across all subjects. The Pearson correlation demonstrated significant reliability for the measurement ($r = 0.89$, $P < 0.001$).

### Between-subject LFP spectral power differences relate to F2 Ratio

We first searched for changes in LFP spectral power that tracked with between session differences in F2 Ratio on a session-by-session basis. Each subject contributed between 2 and 4 sessions of data. We performed a linear fit of z-scored spectral power for each canonical frequency band in a 200 ms window around the onset of vowel production. Once a model was constructed for each brain region of interest, power predictions were calculated to reflect the range of F2 Ratio values present in the data. Predictions of the normalized power were calculated for high F2 Ratio (1.87) and low F2 Ratio (1.05), creating power values for 2 categories of articulatory gain at the extreme values. These values were chosen because they reflect the range of F2 Ratio observed in the data. Spectral pattern differences were observed between high and low F2 Ratio values, with alpha frequency differences predominating in the precentral gyrus and STN (Fig. 4A,B). Sessions with high F2 Ratio tended to have high power in the alpha band, whereas those sessions with a low F2 Ratio exhibited lower alpha band power. Based on this analysis, we concluded that dividing the signal into canonical bands was appropriate for further analysis because differences appeared within canonical band ranges.

### F2 Ratio correlates to cortical alpha and theta power

All available cortical recordings were utilized for this analysis (subject $N = 10$, see Table 2 for corresponding session information). Two mixed effects models were completed on averaged time regions of data: (1) before vowel onset ($t_1 = 1.2$ s before vowel onset to $t_2$ = vowel onset) and (2) during speech production ($t_1$ = vowel onset to $t_2 = 600$ ms after vowel onset (Fig. 5A,B). Time frames were determined by the average speech duration and latency. For both models, the maximal model did not converge, indicating overparameterization of the random effects. The random slope was removed from the model and convergence was achieved with a random intercept of subject. A significant positive main effect of F2 Ratio was found at the time before vowel onset, indicating that F2 Ratio predicted neural power; however, it did not reach statistical significance at the Bonferroni corrected alpha level of 0.0167 ($F_{(4, 111)} = 3.05$, $P_{adj} = 0.03$). For the model during speech production, a significant interaction effect between F2 Ratio and frequency band was found ($F_{(4, 111)} = 5.9$, $P_{adj} < 0.001$), indicating that F2 Ratio predicted neural power, but in only a subset of frequency bands. To determine which bands were responsible for the effect, simple slopes from each band were extracted from the model and this revealed an F2 Ratio effect for alpha (simple slope = 1.44, $P = 0.01$) and theta bands (simple slope = 2.6, $P < 0.001$) (Fig. 5B).

A mixed effect model was conducted before speech onset and during speech production in the postcentral gyrus. Neither time

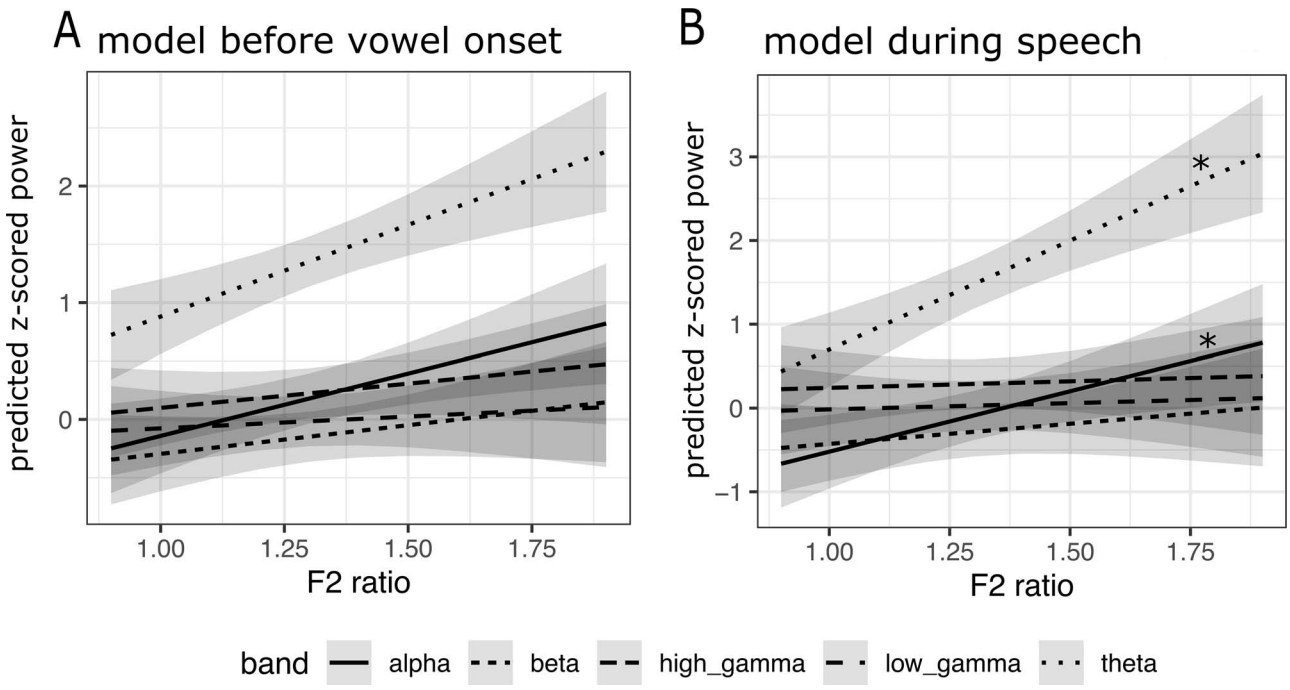


**Figure 5.** F2 Ratio predicts neural power in alpha and theta bands in the precentral gyrus. (A) A mixed effects model predicting neural power from F2 Ratio before vowel onset. Significant main effect of F2 Ratio across all bands was found before correcting for familywise error. (B) A mixed effects model predicting neural power from F2 Ratio during speech production. F2 Ratio by band Interaction effects are shown in panels above, with asterisk indicating a significant simple slope effect. A significant interaction effect was found during speech, but not before vowel onset. *P* values were FDR corrected and a Bonferroni corrected alpha of 0.0167 was utilized to account for familywise error. Gray shaded areas represent confidence intervals for the estimates.

region revealed a significant interaction effect; therefore, post hoc testing was not completed.

### F2 Ratio correlates to subthalamic alpha and theta power

All available STN recordings were utilized for this analysis (subject $N = 11$, see Table 2 for corresponding session information). Two mixed effect models were completed on averaged time regions of data: (1) before vowel onset ($t_1 = 1.2$ s before vowel onset to $t_2 =$ vowel onset) and (2) during speech production ($t_1 =$ vowel onset to $t_2 = 600$ ms after vowel onset) (Fig. 6A,B). For both models, the maximal model converged, and included both a random intercept of subject and random slope of session. No significant interaction effect or main effect was found for the time region before speech onset, indicating no relationship with F2 Ratio. For the time region during speech production, a significant interaction effect between F2 Ratio and frequency band was found ($F_{(4, 112)} = 7.8, P_{adj} < 0.001$) indicating that neural power predicted F2 Ratio, but only in a subset of frequency bands. To determine which bands were responsible for the effect, simple slopes from each band were extracted from the model which revealed a significant predictive relationship for alpha (simple slope = 1.17, $P = 0.001$) and theta power (simple slope = 1.15, $P = 0.0015$) (Fig. 6B).

Significant effects were not driven by disease severity (as measured by UPDRS) or recording location in either the cortex or STN.

### STN-Precentral Beta PLV Correlates to F2 Ratio

We next investigated the effects of the F2 Ratio during speech on STN-cortical functional connectivity by calculating a PLV for each STN-cortical region pair (Equation 6). Correlations were computed on a subject-by-subject basis, rather than by session. Significant correlation between F2 Ratio and average STN-precentral gyrus PLV was observed, with a higher F2 Ratio associated with a lower PLV between STN and precentral gyrus in the beta band (Pearson's $\rho = -0.71$, $P = 0.022$, Fig. 7A). In contrast, subjects' F2 Ratio was not significantly associated with STN-postcentral gyrus beta PLV (Pearson's $\rho = -0.52$, $P = 0.12$, Fig. 7B). PLVs between STN and precentral gyrus and postcentral gyrus in other frequency bands did not significantly correlate to the F2 Ratio. Similarly, correlation analyses excluded the potential effects of UPDRS score, age and the recording depth on STN-cortical PLVs.

## Discussion

These analyses of cortical and STN local field potentials recorded during reading aloud by subjects with Parkinson's disease provide the first description of the neural correlates of articulatory gain in the precentral gyrus and the STN, fundamental nodes in the basal ganglia-thalamocortical motor control circuit. These findings build on our previous work, describing concurrent involvement of the STN and motor cortex during speech that is specific to certain articulator features (Chrabaszcz et al. 2019). The present study provides additional insight into how speech may be modulated by activity in the basal ganglia-thalamocortical loop. We found that naturally occurring differences in articulatory gain were correlated with normalized alpha and theta power in both the precentral gyrus and the STN. No relationships between articulatory gain and normalized power were observed for any spectral band in postcentral gyrus, despite evidence for

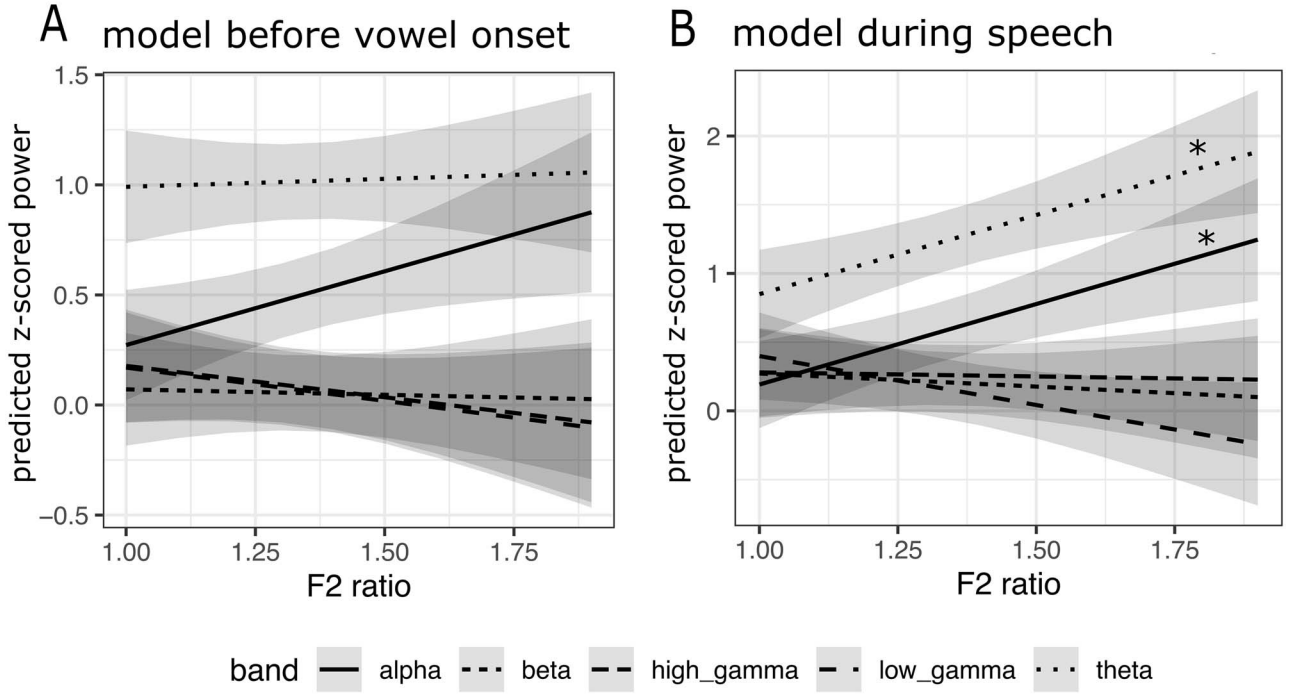


**Figure 6.** F2 Ratio predicts neural power in alpha and theta band in subthalamic nucleus. (*A*) A mixed effects model predicting neural power from F2 Ratio and band was fit in an averaged time window before vowel onset. (*B*) A mixed effects model predicting neural power from F2 Ratio and band was fit in an averaged time window during speech production. F2 Ratio by band Interaction effects are shown in panels above, with asterisk indicating a significant effect after corrections for multiple comparisons both within brain region and across regions. A significant interaction effect was found during speech, but not before vowel onset. *P* values were FDR corrected and a Bonferroni corrected alpha of 0.0167 was utilized to account for familywise error. Gray shaded areas represent confidence intervals for the estimates.

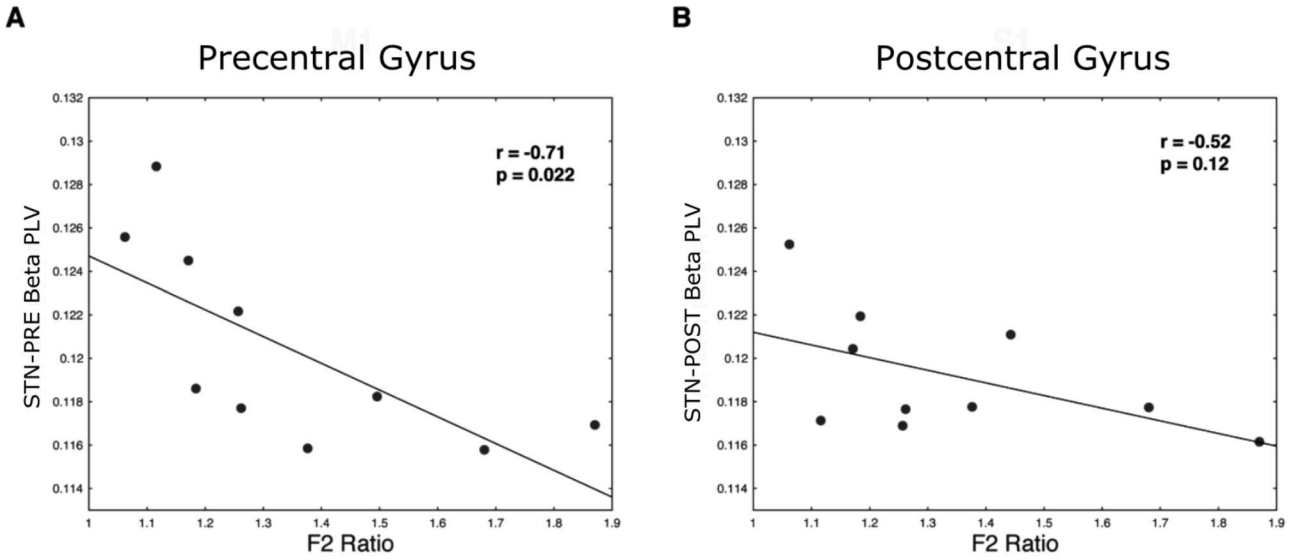


**Figure 7.** STN-Precentral gyrus beta functional connectivity as measured by phase locking value correlates to F2 Ratio. (A) Subjects' F2 Ratios are plotted against the average STN-precentral gyrus beta PLVs. (*B*) Subjects' F2 Ratios are plotted against the average STN-postcentral gyrus beta PLVs.

STN-sensory cortex information transfer during handgrip force generation (Lipski et al. 2017; Alhourani et al. 2020). Importantly, Parkinson's disease subjects with less-differentiated speech production (lower articulatory gain) demonstrated greater functional connectivity between the STN and precentral gyrus in the beta band, consistent with idea that hypersynchronous oscillations in this frequency band are related to bradykinetic symptoms (Wichmann 2019). Together, these data suggest that the precentral gyrus and STN participate in a network that modulates articulatory gain.

## Articulatory Gain Representation in the Precentral Gyrus

The precentral gyrus is an important modulator of articulatory gain. Articulator somatotopic organization of neural activity in

the precentral gyrus is well established (Blakely et al. 2008; Conant et al. 2014; Breshears et al. 2015; Chrabaszcz et al. 2019;). We found that power in alpha and theta frequencies was positively correlated with the F2 Ratio. Alpha power demonstrated a nearly identical positive relationship with articulatory gain before and during vowel onset (Fig. 5A,B), suggesting that it is not unique to motor execution of articulatory gain. Alpha band activity may also reflect supportive processes, such as inhibition of competing motor programs (Brinkman et al. 2014). Theta oscillations have been proposed to play a significant role in the neural processing that supports speech perception, serving to "parse" the speech envelope and encode linguistic units at the syllable level (Giraud and Poeppel 2012). Stimuli used in this study consisted of single syllable units, supporting the idea that modulations in articulatory gain occurring at the syllable level are encoded in theta frequencies. Theta activity has also been implicated in feedforward adaptive control of vowel production (Sengupta and Nasir 2015, 2016).

It was surprising that gamma frequencies did not demonstrate a relationship with articulatory gain because high-frequency activity has been proposed to be modulated by the phase of theta frequencies in speech production tasks (Doesburg et al. 2012), has been described as integral to speech processing (Giraud and Poeppel 2012) and has an established role for articulatory kinematics in the cortex (Riecker et al. 2000; Pulvermuller et al. 2006; Chartier et al. 2018).

## Articulatory Gain Representation in STN

Evidence that the basal ganglia modulates articulatory gain includes observations of hypo or hyperkinetic speech effects associated with basal ganglia lesions (Murdoch 2001), Huntington's chorea (Hartelius et al. 2003), and Parkinson's disease (Logemann et al. 1978). In addition, STN DBS has been shown to reduce articulatory vowel space area (Martel Sauvageau et al. 2015), an alternative acoustic indicator of articulatory gain (Sapir et al. 2010), and STN DBS can be associated with improvement in voice function (Jorge et al. 2020). Our results add electrophysiological evidence that the STN participates in aspects of articulatory gain, via synchronization of neural activity in theta and alpha bands. Effects found in the STN occurred exclusively during speech production, in line with the concept that the basal ganglia contributes to the online modulation of movement (Tunik et al. 2009). The distinct positive shift in the theta band relationship with articulatory gain from prevowel, flat slope, to a clearly positive relationship during vowel production (Fig. 6), further highlights the importance of the STN during movement.

As in the precentral gyrus, STN alpha power was positively correlated with the F2 Ratio. Interestingly, one of the few previous studies to focus on alpha activity in the basal ganglia found that complex fast arm movements cause synchronized activity in the STN in the alpha frequency range, but slow repetitive active or passive movements did not (Singh et al. 2011). Alpha activity, therefore, may be required to sustain more complex motor plans, like speech production. A positive relationship was also found between theta band power and articulatory gain. This finding warrants future exploration, given the potential role of theta oscillations in speech perception (Giraud and Poeppel 2012) and the proposed role of subthalamic theta oscillations in cortical monitoring (Zavala et al. 2016).

## Articulatory Gain Representation in the BG-Cortical Circuit

These articulatory gain-related power changes observed during simultaneous recording of the precentral gyrus and STN activity suggest that the basal ganglia and motor cortex are linked in a speech production network (Murdoch 2001; Bohland et al. 2010; Lipski et al. 2018; Chrabaszcz et al. 2019). Correlations between individual frequency bands and articulatory gain occurred earlier in the precentral gyrus compared to STN. Relationships in the precentral gyrus occurred prior to movement onset and during speech production (alpha and theta bands), whereas the relationships in the STN only occurred during speech production. To investigate cortical-STN functional connectivity directly, we examined the relationship of oscillation phases between the STN and cortex. Phase locking of beta oscillations between the precentral gyrus and STN was the only connectivity measure found to correlate with articulatory gain, demonstrating an inverse correlation with speech gain in each location. Increases in a similar connectivity measure, coherence between motor regions, has been attributed to motor planning, with lower coherence expected during motor execution (Yeom et al. 2020); therefore our results of low PLV connectivity related to high articulatory gain may reflect processes occurring primarily during motor execution. This interpretation is also consistent with the timing of the alpha and theta band effects, which demonstrated the most robust F2 Ratio effects during speech production. Excessive synchronization between cortical and subcortical regions during execution may be detrimental to optimal speech motor performance. In general, desynchronization processes in beta band have been linked to a release from maintenance of a static behavior (Engel and Fries 2010; Lipski et al. 2017; Holt et al. 2019; Alhourani et al. 2020), previously shown to occur with speech production (Hebb et al. 2012; Lipski et al. 2018; Chrabaszcz et al. 2019).

Interestingly, in contrast to our previous studies of hand grip force generation, where patterns of STN unit firing (Lipski et al. 2017) and local field potential activity (Alhourani et al. 2020) indicated the flow of information between the STN and parietal sensory cortex during movement, no relationship was found between articulatory gain and activity in postcentral gyrus or STN-postcentral gyrus functional connectivity. This finding is surprising, as the postcentral gyrus is known to receive information regarding motor output (Umeda et al. 2019), which seems likely be important for articulatory gain. However, the F2 Ratio measures formant frequency information, which is largely driven by changes in tongue position (Fig. 2), and the electrode contacts in the postcentral gyrus may not have provided sufficient coverage of the tongue sensory cortex (Bouchard et al. 2013; Chrabaszcz et al. 2019) for signal detection.

## Limitations

Anatomical specificity of the articulatory gain relationships was limited by the behavioral calculations of the F2 Ratio. Patterns in individual electrodes could not be analyzed because the F2 Ratio calculations were only possible at the session level, not within trials, which prevented a within-subject single electrode analysis. It was necessary to average data at the session level to mitigate confounds of phonetic context on the primary outcome variable, the F2 Ratio. Our study was conducted in patients with Parkinson's disease, which is known to affect articulatory gain performance. Although disease severity did not explain

the relationship found between the F2 Ratio and neural power, it is possible that abnormal neural synchrony due to Parkinson's disease influences these relationships. These results also represent between-subject effects, which can be influenced by intersubject differences.

### Conclusions

Our data suggest that speech gain is represented in neural activity of the basal ganglia-thalamo-cortical network. Patients with high F2 Ratio, and therefore high articulatory gain, demonstrated positive relationships in low frequencies, alpha and theta bands. Articulatory gain relationships began earlier in the precentral gyrus, beginning "before movement", whereas correlated activity in the STN exclusively occurred "during movement", when low levels of beta connectivity between the precentral gyrus and STN were correlated with better articulatory gain. These rhythms may reflect a framework in which cortical areas prepare motor plans to optimize articulatory gain, and the STN participates in modulation of these commands via activity in alpha and theta bands within the basal ganglia-cortical loop.

## Supplementary Material

Supplementary material can be found at *Cerebral Cortex* online.

## Funding

National Institute of Neurological Disorders and Stroke, National Institute of Health (U01NS098969 and F31DC01903401A1). The University of Pittsburgh-Tsinghua University Scholars Program (to D.W.).

## Notes

We are indebted to our patient-participants. *Conflict of Interest:* None declared.

## References

Aldridge D, Theodoros D, Angwin A, Vogel AP. 2016. Speech outcomes in Parkinson's disease after subthalamic nucleus deep brain stimulation: a systematic review. *Parkinsonism Relat Disord*. 33:3–11. https://doi.org/10.1016/j.parkreldis.2016.09.022.

Alhourani A, Korzeniewska A, Wozny TA, Lipski WJ, Kondylis ED, Ghuman AS, Crone NE, Crammond DJ, Turner RS, Richardson RM. 2020. Subthalamic Nucleus Activity Influences Sensory and Motor Cortex during Force Transduction. *Cereb Cortex*. https://doi.org/10.1093/cercor/bhz264.

Brainard DH. 1997. The Psychophysics Toolbox. *Spat Vis*. 10:433–436.

Behroozmand R, Johari K, Greenlee MD. 2018. *Effect of STN-DBS on sensorimotor integration mechanisms of voice motor control in Parkinson's disease*. San Diego, CA: Society for Neuroscience.

Behroozmand R, Shebek R, Hansen DR, Oya H, Robin DA, Howard MA 3rd, Greenlee JD. 2015. Sensory-motor networks involved in speech production and motor control: an fMRI study. *Neuroimage*. 109:418–428. https://doi.org/10.1016/j.neuroimage.2015.01.040.

Benjamini Y, Yekutieli D. 2001. The control of the false discovery rate in multiple testing under dependency. *Ann. Statist*. 29(4):1165–1188.

Blakely T, Miller KJ, Rao RP, Holmes MD, Ojemann JG. 2008. Localization and classification of phonemes using high spatial resolution electrocorticography (ECoG) grids. *Annu Int Conf IEEE Eng Med Biol Soc*. 2008:4964–4967. https://doi.org/10.1109/IEMBS.2008.4650328.

Boersma, P., & Weenink, D. (2019). *Praat: doing phonetics by computer [Computer program]. In* (Version 6.0.50). http://www.praat.org

Bohland JW, Bullock D, Guenther FH. 2010. Neural representations and mechanisms for the performance of simple speech sequences. *J Cogn Neurosci*. 22(7):1504–1529. https://doi.org/10.1162/jocn.2009.21306.

Bouchard KE, Chang EF. 2014a. Control of spoken vowel acoustics and the influence of phonetic context in human speech sensorimotor cortex. *J Neurosci*. 34(38):12662–12677. https://doi.org/10.1523/JNEUROSCI.1219-14.2014.

Bouchard KE, Chang EF. 2014b. Neural decoding of spoken vowels from human sensory-motor cortex with high-density electrocorticography. *Conf Proc IEEE Eng Med Biol Soc*. 2014:6782–6785. https://doi.org/10.1109/EMBC.2014.6945185.

Bouchard KE, Conant DF, Anumanchipalli GK, Dichter B, Chaisanguanthum KS, Johnson K, Chang EF. 2016. High-Resolution, Non-Invasive Imaging of Upper Vocal Tract Articulators Compatible with Human Brain Recordings. *PLoS One*. 11(3):e0151327. https://doi.org/10.1371/journal.pone.0151327.

Bouchard KE, Mesgarani N, Johnson K, Chang EF. 2013. Functional organization of human sensorimotor cortex for speech articulation. *Nature*. 495(7441):327–332. https://doi.org/10.1038/nature11911.

Breshears JD, Molinaro AM, Chang EF. 2015. A probabilistic map of the human ventral sensorimotor cortex using electrical stimulation. *J Neurosurg*. 123(2):340–349. https://doi.org/10.3171/2014.11.JNS14889.

Brinkman L, Stolk A, Dijkerman HC, de Lange FP, Toni I. 2014. Distinct roles for alpha- and beta-band oscillations during mental simulation of goal-directed actions. *J Neurosci*. 34(44):14783–14792. https://doi.org/10.1523/JNEUROSCI.2039-14.2014.

Chartier J, Anumanchipalli GK, Johnson K, Chang EF. 2018. Encoding of articulatory kinematic trajectories in human speech sensorimotor cortex. *Neuron*. 98(5):1042–1054e1044. https://doi.org/10.1016/j.neuron.2018.04.031.

Chladkova K, Escudero P, Boersma P. 2011. Context-specific acoustic differences between Peruvian and Iberian Spanish vowels. *J Acoust Soc Am*. 130(1):416–428. https://doi.org/10.1121/1.3592242.

Chrabaszcz A, Neumann WJ, Stretcu O, Lipski WJ, Bush A, Dastolfo-Hromack C, Wang D, Crammond DJ, Shaiman S, Dickey MW, et al. 2019. Subthalamic nucleus and sensorimotor cortex activity during speech production. *J Neurosci*. . https://doi.org/10.1523/JNEUROSCI.2842-18.2019.

Conant D, Bouchard KE, Chang EF. 2014. Speech map in the human ventral sensory-motor cortex. *Curr Opin Neurobiol*. 24(1):63–67. https://doi.org/10.1016/j.conb.2013.08.015.

R Core Team 2018. *R: A language and environment for statistical omputing*. R Foundation for Statistical Computing, Vienna, Austria. URL https://www.R-project.org/.

Crone NE, Miglioretti DL, Gordon B, Lesser RP. 1998. Functional mapping of human sensorimotor cortex with electrocorticographic spectral analysis. *II. Event-related synchronization in the gamma band. Brain*. 121(Pt 12):2301–2315. https://doi.org/10.1093/brain/121.12.2301.

Dale AM, Fischl B, Sereno MI. 1999. Cortical surface-based analysis. *I. Segmentation and surface reconstruction*. *Neuroimage*. 9(2):179–194. https://doi.org/10.1006/nimg.1998.0395.

Doesburg SM, Vinette SA, Cheung MJ, Pang EW. 2012. Theta-modulated gamma-band synchronization among activated regions during a verb generation task. *Front Psychol*. 3:195. https://doi.org/10.3389/fpsyg.2012.00195.

Eickhoff SB, Heim S, Zilles K, Amunts K. 2009. A systems perspective on the effective connectivity of overt speech production. *Philos Trans A Math Phys Eng Sci*. 367(1896):2399–2421. https://doi.org/10.1098/rsta.2008.0287.

Engel AK, Fries P. 2010. Beta-band oscillations–signalling the status quo? *Curr Opin Neurobiol*. 20(2):156–165. https://doi.org/10.1016/j.conb.2010.02.015.

Eusebio A, Brown P. 2009. Synchronisation in the beta frequency-band–the bad boy of parkinsonism or an innocent bystander? *Exp Neurol*. 217(1):1–3. https://doi.org/10.1016/j.expneurol.2009.02.003.

Giraud AL, Poeppel D. 2012. Cortical oscillations and speech processing: emerging computational principles and operations. *Nat Neurosci*. 15(4):511–517. https://doi.org/10.1038/nn.3063.

Guenther FH. 2015. *Neural control of speech*. Cambridge, MA: The MIT Press.

Hartelius L, Carlstedt A, Ytterberg M, Lillbik M, Laakso K. 2003. Speech disorders in mild and moderate Huntington's disease: results of dysarthria assessments of 19 individuals. *J Med Speech Lang Pathol*. 11(1):1–14.

Hebb AO, Darvas F, Miller KJ. 2012. Transient and state modulation of beta power in human subthalamic nucleus during speech production and finger movement. *Neuroscience*. 202:218–233. https://doi.org/10.1016/j.neuroscience.2011.11.072.

Hickok G. 2012. Computational neuroanatomy of speech production. *Nat Rev Neurosci*. 13(2):135–145. https://doi.org/10.1038/nrn3158.

Hillenbrand JM, Clark MJ, Nearey TM. 2001. Effects of consonant environment on vowel formant patterns. *J Acoust Soc Am*. 109(2):748–763. https://doi.org/10.1121/1.1337959.

Hohlefeld FU, Ewald A, Ehlen F, Tiedt HO, Horn A, Kuhn AA, Curio G, Klostermann F, Nikulin VV. 2017. Neural correlates of lexical decisions in Parkinson's disease revealed with multivariate extraction of cortico-subthalamic interactions. *Clin Neurophysiol*. 128(4):538–548. https://doi.org/10.1016/j.clinph.2016.12.026.

Horn A, Kuhn AA. 2015. Lead-DBS: a toolbox for deep brain stimulation electrode localizations and visualizations. *Neuroimage*. 107:127–135.

Holt AB, Kormann E, Gulberti A, Potter-Nerger M, McNamara CG, Cagnan H, Baaske MK, Little S, Koppen JA, Buhmann C, et al. 2019. Phase-Dependent Suppression of Beta Oscillations in Parkinson's Disease Patients. *J Neurosci*. 39(6):1119–1134. https://doi.org/10.1523/JNEUROSCI.1913-18.2018.

Houde JF, Nagarajan SS. 2011. Speech production as state feedback control. *Front Hum Neurosci*. 5:82. https://doi.org/10.3389/fnhum.2011.00082.

Jorge A, Dastolfo-Hromack C, Lipski WJ, Kratter IH, Smith LJ, Gartner-Schmidt JL, Richardson RM. 2020. Anterior sensorimotor subthalamic nucleus stimulation is associated with improved voice function. *Neurosurgery*. 87(4):788–795. https://doi.org/10.1093/neuros/nyaa024.

Kent R, Read C. 2002. *The acoustic analysis of speech*. Albany, NY: Singular/Thomson Learning.

Kent RD, Weismer G, Kent JF, Vorperian HK, Duffy JR. 1999. Acoustic studies of dysarthric speech: methods, progress, and potential. *J Commun Disord*. 32(3):141–180183-146; quiz 181-143, 187-149. https://doi.org/10.1016/s0021-9924(99)00004-0.

Kleiner M, Brainard D, Pelli D, Ingling A, Murray R, Broussard C. 2007. What's new in 382 psychtoolbox-3. *Perception*. 36:1–16.

Kriegeskorte N, Simmons WK, Bellgowan PS, Baker CI. 2009. Circular analysis in systems neuroscience: the dangers of double dipping. *Nat Neurosci*. 12(5):535–540. https://doi.org/10.1038/nn.2303.

Lachaux JP, Rodriguez E, Martinerie J, Varela FJ. 1999. Measuring phase synchrony in brain signals. *Hum Brain Mapp*. 8(4):194–208. https://doi.org/10.1002/(sici)1097-0193(1999)8:4<194::aid-hbm4>3.0.co;2-c.

Lee M, van Santen J, Mobius B, Olive J. 2005. Formant tracking using context-dependent phonemic information. *IEEE Trans Speech Audio Process*. 13(5):741–750.

Lipski WJ, Alhourani A, Pirnia T, Jones PW, Dastolfo-Hromack C, Helou LB, Crammond DJ, Shaiman S, Dickey MW, Holt LL, et al. 2018. Subthalamic nucleus neurons differentially encode early and late aspects of speech production. *J Neurosci*. 38(24):5620–5631. https://doi.org/10.1523/JNEUROSCI.3480-17.2018.

Lipski WJ, Wozny TA, Alhourani A, Kondylis ED, Turner RS, Crammond DJ, Richardson RM. 2017. Dynamics of human subthalamic neuron phase-locking to motor and sensory cortical oscillations during movement. *J Neurophysiol*. 118(3):1472–1487. https://doi.org/10.1152/jn.00964.2016.

Little S, Bonaiuto J, Barnes G, Bestmann S. 2019. Human motor cortical beta bursts relate to movement planning and response errors. *PLoS Biol*. 17(10):e3000479. https://doi.org/10.1371/journal.pbio.3000479.

Lofredi R, Neumann WJ, Bock A, Horn A, Huebl J, Siegert S, Schneider GH, Krauss JK, Kuhn AA. 2018. Dopamine-dependent scaling of subthalamic gamma bursts with movement velocity in patients with *Parkinson's disease*. *Elife*. 7. https://doi.org/10.7554/eLife.31895.

Logemann JA, Fisher HB, Boshes B, Blonsky ER. 1978. Frequency and cooccurrence of vocal tract dysfunctions in the speech of a large sample of Parkinson patients. *J Speech Hear Disord*. 43(1):47–57. https://www.ncbi.nlm.nih.gov/pubmed/633872.

Martel Sauvageau V, Roy JP, Cantin L, Prud'Homme M, Langlois M, Macoir J. 2015. Articulatory changes in vowel production following STN DBS and Levodopa intake in Parkinson's disease. *Parkinsons Dis*. 2015:382320. https://doi.org/10.1155/2015/382320.

MATLAB. 2017. *9.7.0.1190202 (R2017a)*. Natick, Massachusetts: The MathWorks Inc.

Matuschek H *et al*. 2017. Balancing Type I error and power in linear mixed models. *Journal of Memory and Language*. 94:305–315.

Moore MW, Fiez JA, Tompkins CA. 2017. Consonant age-of-acquisition effects in nonword repetition are not articulatory in nature. *J Speech Lang Hear Res*. 60(11):3198–3212.

Murdoch BE. 2001. Subcortical brain mechanisms in speech and language. *Folia Phoniatr Logop*. 53(5):233–251. https://doi.org/10.1159/000052679.

Oostenveld R *et al*. 2011. FieldTrip: Open source software for advanced analysis of MEG, EEG, and invasive electrophysiological data. *Comput Intell Neurosci*. 156869.

Pelli DG. 1997. The VideoToolbox software for visual psychophysics. *Spatial Vision*. 10:437–442.

Panov F, Levin E, de Hemptinne C, Swann NC, Qasim S, Miocinovic S, Ostrem JL, Starr PA. 2017. Intraoperative electrocorticography for physiological research in movement disorders: principles and experience in 200 cases. *J Neurosurg*. 126(1):122–131. https://doi.org/10.3171/2015.11.JNS151341.

Perkell J. 2012. Movement goals and feedback and feedforward control mechanisms in speech production. *J Neurolinguist*. 25(5):382–407. https://doi.org/10.1016/j.jneuroling.2010.02.011.

Perkell J, Matthies M, Lane H, Guenther F, Wilhelms-Tricarico R, Wozniak J, Guiod P. 1997. Speech motor control: acoustic goals, saturation effects, auditory feedback and internal models. *Speech Commun*. 22:227–250.

Pulvermuller F, Huss M, Kherif F, Moscoso del Prado Martin F, Hauk O, Shtyrov Y. 2006. Motor cortex maps articulatory features of speech sounds. *Proc Natl Acad Sci U S A*. 103(20):7865–7870. https://doi.org/10.1073/pnas.0509989103.

Randazzo MJ, Kondylis ED, Alhourani A, Wozny TA, Lipski WJ, Crammond DJ, Richardson RM. 2016. Three-dimensional localization of cortical electrodes in deep brain stimulation surgery from intraoperative fluoroscopy. *Neuroimage*. 125:515–521. https://doi.org/10.1016/j.neuroimage.2015.10.076.

Ray S, Niebur E, Hsiao SS, Sinai A, Crone NE. 2008. High-frequency gamma activity (80-150Hz) is increased in human cortex during selective attention. *Clin Neurophysiol*. 119(1):116–133. https://doi.org/10.1016/j.clinph.2007.09.136.

Riecker A, Ackermann H, Wildgruber D, Meyer J, Dogil G, Haider H, Grodd W. 2000. Articulatory/phonetic sequencing at the level of the anterior perisylvian cortex: a functional magnetic resonance imaging (fMRI) study. *Brain Lang*. 75(2):259–276. https://doi.org/10.1006/brln.2000.2356.

Sapir S. 2014. Multiple factors are involved in the dysarthria associated with Parkinson's disease: a review with implications for clinical practice and research. *J Speech Lang Hear Res*. 57(4):1330–43. https://doi.org/10.1044/2014_JSLHR-S-13-0039.

Sapir S, Ramig LO, Spielman JL, Fox C. 2010. Formant centralization ratio: a proposal for a new acoustic measure of dysarthric speech. *J Speech Lang Hear Res*. 53(1):114–125. https://doi.org/10.1044/1092-4388(2009/08-0184).

Sapir S, Spielman JL, Ramig LO, Story BH, Fox C. 2007. Effects of intensive voice treatment (the Lee Silverman Voice Treatment [LSVT]) on vowel articulation in dysarthric individuals with idiopathic Parkinson disease: acoustic and perceptual findings. *J Speech Lang Hear Res*. 50(4):899–912. https://doi.org/10.1044/1092-4388(2007/064).

Sengupta R, Nasir SM. 2015. Redistribution of neural phase coherence reflects establishment of feedforward map in speech motor adaptation. *J Neurophysiol*. 113(7):2471–2479. https://doi.org/10.1152/jn.00731.2014.

Sengupta R, Nasir SM. 2016. The predictive roles of neural oscillations in speech motor adaptability. *J Neurophysiol*. 115(5):2519–2528. https://doi.org/10.1152/jn.00043.2016.

Singh A, Levin J, Mehrkens JH, Botzel K. 2011. Alpha frequency modulation in the human basal ganglia is dependent on motor task. *Eur J Neurosci*. 33(5):960–967. https://doi.org/10.1111/j.1460-9568.2010.07577.x.

Sisterson ND, Carlson AA, Rutishauser U, Mamelak AN, Flagg M, Pouratian N, Salimpour Y, Anderson WS, Richardson RM. 2021. Electrocorticography during deep brain stimulation surgery: safety experience from 4 centers within the national institute of neurological disorders and stroke research opportunities in human consortium. *Neurosurgery*. https://doi.org/10.1093/neuros/nyaa592.

Slis A, Van Lieshout P. 2013. The effect of phonetic context on speech movements in repetitive speech. *J Acoust Soc Am*. 134(6):4496. https://doi.org/10.1121/1.4828834.

Soros P, Sokoloff LG, Bose A, McIntosh AR, Graham SJ, Stuss DT. 2006. Clustered functional MRI of overt speech production. *Neuroimage*. 32(1):376–387. https://doi.org/10.1016/j.neuroimage.2006.02.046.

Stevens KN, House AS. 1963. Perturbation of vowel articulations by consonantal context: an acoustical study. *J Speech Hear Res*. 6:111–128. https://doi.org/10.1044/jshr.0602.111.

Strange W, Weber A, Levy ES, Shafiro V, Hisagi M, Nishi K. 2007. Acoustic variability within and across German, French, and American English vowels: phonetic context effects. *J Acoust Soc Am*. 122(2):1111–1129. https://doi.org/10.1121/1.2749716.

Tadel F, Baillet S, Mosher JC, Pantazis D, Leahy RM. 2011. Brainstorm: a user-friendly application for MEG/EEG analysis. *Comput Intell Neurosci*. 2011:879716. https://doi.org/10.1155/2011/879716.

Tankus A, Fried I. 2019. Degradation of neuronal encoding of speech in the subthalamic nucleus in Parkinson's disease. *Neurosurgery*. 84(2):378–387. https://doi.org/10.1093/neuros/nyy027.

Tankus A, Mirelman A, Giladi N, Fried I, Hausdorff JM. 2018. Pace of movement: the role of single neurons in the subthalamic nucleus. *J Neurosurg*. 1–6. https://doi.org/10.3171/2018.1.JNS171859.

Tunik E, Houk JC, Grafton ST. 2009. Basal ganglia contribution to the initiation of corrective submovements. *Neuroimage*. 47(4):1757–1766. https://doi.org/10.1016/j.neuroimage.2009.04.077.

Turner RS, Desmurget M. 2010. Basal ganglia contributions to motor control: a vigorous tutor. *Curr Opin Neurobiol*. 20(6):704–716. https://doi.org/10.1016/j.conb.2010.08.022.

Umeda T, Isa T, Nishimura Y. 2019. The somatosensory cortex receives information about motor output. *Sci Adv*. 5(7):eaaw5388. https://doi.org/10.1126/sciadv.aaw5388.

Wichmann T. 2019. Changing views of the pathophysiology of Parkinsonism. *Mov Disord*. 34(8):1130–1143. https://doi.org/10.1002/mds.27741.

Yeom HG, Kim JS, Chung CK. 2020. Brain mechanisms in motor control during reaching movements: transition of functional connectivity according to movement states. *Sci Rep*. 10(1):567. https://doi.org/10.1038/s41598-020-57489-7.

Zavala B, Tan H, Ashkan K, Foltynie T, Limousin P, Zrinzo L, Zaghloul K, Brown P. 2016. Human subthalamic nucleus-medial frontal cortex theta phase coherence is involved in conflict and error related cortical monitoring. *Neuroimage*. 137:178–187. https://doi.org/10.1016/j.neuroimage.2016.05.031.